RSC Advances

PAPER

Cite this: *RSC Adv.*, 2022, **12**, 5677

Fabrication and functionalization of biocompatible carboxymethyl chitosan/gelatin membranes *via* anodic electrophoretic deposition

Fushi Wang,†[ab] Weiwei Qiao,†[ab] Weiting Guo,[a] Zhiwen Li[c] and Xinjie Cai *[ad]

Peri-implant surgical site infection is a significant challenge in oral implant surgery. Numerous surface functionalization methods, including electrophoretic deposition, have been studied to functionalize implant surfaces to prevent peri-implantitis. However, it is still challenging to load anti-inflammatory agents having negative charges into electrophoretic deposition membranes. The present study aimed to use water-soluble chitosan derivatives to fabricate negatively charged carboxymethyl chitosan/gelatin (CMCG) composite membranes on titanium (Ti) substrates *via* anodic electrophoretic deposition (AED). Membranes incorporating different amounts of gelatin were labeled as CMC, CMCG4, CMCG6, and CMCG8. X-ray diffraction and Fourier transform infrared spectroscopy tests verified that CMCG could be deposited on Ti disks *via* AED. The result of the contact angle test showed that groups incorporating gelatin had a certain degree of hydrophobicity. After rehydration, the membranes swelled by approximately 200% in weight. Fluorescence microscopy and scanning electron microscopy images showed that bone marrow stromal cells (BMSCs) on membranes stretched well, showing a good cell adhesion ability. The CCK-8 test demonstrated that CMCG6 had the highest proliferation rate. Cell apoptosis studies showed that CMCG could inhibit apoptosis of BMSCs statistically. It suggests that the CMCG membrane fabricated by AED would be a potent candidate for surface functionalization of biomaterials with negative charges.

Received 21st December 2021
Accepted 5th February 2022

DOI: 10.1039/d1ra09231f

rsc.li/rsc-advances

1. Introduction

Peri-implant surgical site infection, also known as peri-implantitis, is a severe complication in oral implant surgery and orthopedic surgery. According to literature reports, 18.5% of patients and 12.8% of implants were afflicted by inflammation around the implant.[1] In orthopedics, even under strict aseptic surgical procedures, 5–33% of patients with implants developed acute infections or chronic osteomyelitis.[2] The causes of infection in oral implants can be mainly attributed to the formation of bacterial biofilms on the surface of implants and the decreased immunity of the integrated interface between the endosseous implant and bone tissues.[3] Applications of antibiotics before and during routine surgery cannot completely prevent infections. Once bacterial biofilms are formed, it is challenging to achieve therapeutic effects with conventional types and doses of antibiotics.[4] Regarding the treatment of peri-implantitis, once the inflammation around the implant occurs, it is inevitable that the implant must be removed, anti-infection treatment provided, bone loss prevented, bone regeneration induced, and then implant surgery performed at an optional time for radical cure.[5] Consequently, it is essential to load antibacterial and osteogenesis-promoting agents into the peri-implant sites.

To modify the surface of the implants and control the infection, surface functionalization was introduced to create biomimetic niches, that could regulate peri-implant stem cells and enhance cellular functions.[6] Surface functionalization was made up of physical adsorption,[7] the Langmuir Blodgett method,[8] ion beam deposition,[9] self-assembled monolayer,[10] plasma treatment,[11] and other physical or chemical techniques. Despite some advantages, such as efficiency, several weaknesses of these strategies, for instance, relatively high cost and time-consuming, still constrain their applications. For these reasons, it was proposed that chitosan/gelatin (CS/G) nanocomposite membrane prepared by the method of electrophoretic deposition (EPD) could functionalize titanium (Ti) surfaces.[12] Such membranes could introduce some osteogenic or antibacterial agents onto Ti substrates in moderate conditions (such as room temperature with water as the solvent).[13]

[a]*The State Key Laboratory Breeding Base of Basic Science of Stomatology (Hubei-MOST), Key Laboratory of Oral Biomedicine Ministry of Education, School and Hospital of Stomatology, Wuhan University, Wuhan 430079, People's Republic of China. E-mail: xinjie.cai@whu.edu.cn*

[b]*Department of Cariology and Endodontics, Hospital of Stomatology, Wuhan University, Wuhan 430079, People's Republic of China*

[c]*College of Geography and Environmental Sciences, Zhejiang Normal University, Jinhua 321004, People's Republic of China*

[d]*Department of Prosthodontics, Hospital of Stomatology, Wuhan University, Wuhan 430079, People's Republic of China*

† These authors contributed equally to this work.

Because of the constraint of the electric charge of chitosan molecules, the method of EPD we previously used was mainly referred to as cathodic electrophoretic deposition (CED),[12] which signified that it was difficult to deposit some macromolecules or ions with negative charges. The applications of chitosan also have severe limitations since it is insoluble in a neutral pH environment because of its relatively stable structure due to strong hydrogen bonds. Moreover, it has been reported that negatively charged surfaces could reduce bacterial adhesion and biofilm formation more efficiently because bacterial membranes are negatively charged.[14] Therefore, to improve the solubility and change the chitosan charge, its depolymerized derivatives, such as carboxymethyl chitosan (CMC), came to our attention. As a water-soluble chitosan derivative, CMC could adsorb metal ions, deliver drugs, heal wounds, and other biomedical activities.[15] We speculated that CMC's macromolecules that carry negative charges could load some small negative molecules or ions and be applied in anodic electrophoretic deposition (AED), as long as these conditions are met: the electric field force on the small molecule and the intermolecular force between the small molecule and the CMC are greater than the repulsive force between the small molecule and the CMC with the same charge. It has been reported that AED could deposit cellulose nanocrystals/alginate composite.[16] Therefore, here we assumed that CMC could be used in the process of AED. In addition, gelatin was introduced to enhance the cell affinity for chitosan/gelatin membranes.[12]

In general, we deposited CMC and gelatin *via* AED to functionalize the surface of biomedical Ti substrates, thereby carrying agents with negative charges on the composite membranes. The surface morphology, physicochemical properties, and cytological studies of the membranes we fabricated were also analyzed.

2. Experimental

2.1. Materials

CMC (carboxylation degree >80%) was supplied by Yuanye Biotechnology (China). Gelatin was procured from Sigma-Aldrich (Type B, Switzerland). Grade 2 pure Ti disks were purchased from Baoji Titanium Industry, China. Other common agents were analytical-grade products obtained from Sinopharm Chemical Reagent Co., Ltd (China).

2.2. Preparation of CMC stock solution

The CMC stock solution prepared was similar to that in our group's previous study.[12] In detail, 8.0 g CMC was dissolved in 480 mL Milli-Q water and stirred until completely dissolved. Then, 0.1 M hydrochloric acid was added to alter the pH of the mixture to 8.00. Subsequently, the solution was filtrated with a filter (0.45 μm), and the solution was constant to 500 mL with a volumetric flask. The CMC solution was then stocked at 4 °C.

2.3. Process of AED

Before the AED, as in our previous work introduced,[13] Ti disks were blasted with 0.05–0.25 mm corundum grits and treated with an isometric hydrochloric acid/sulfuric acid mixture at 60 °C for 1 h. Then, anhydrous acetone, ethanol, and Milli-Q water were used to clean the disks ultrasonically, respectively. Variable weights of gelatin (0, 0.8, 1.2, and 1.6 g) were dissolved in 20 mL CMC solution at 60 °C to form the AED solution. These groups were labeled CMC, CMCG4, CMCG6, and CMCG8, respectively. Meanwhile, the negative control group was marked as pure Ti. The pH of each AED solution was detected by the digital pH meter (FE20, Mettler Toledo, Switzerland).

To perform the AED, a Ti disk and a platinum foil were assigned as the anode and the cathode, respectively. Next, the deposition process was implemented by a power source (Model 6614C, Agilent, USA) and finished after 2 minutes at 20 mA. Disks were then rinsed and dried at room temperature.

2.4. Characterization of the membranes

2.4.1. Surface characterization. Fluorescence microscopy (TE-2000, Nikon, Japan) equipped with a charge-coupled device camera (Diagnostic Instruments, USA) was used to observe the fluorescence images of the samples. The scanning electron microscope (SEM, Zeiss SIGMA, Germany) was used to investigate the surface morphology of every sample. A Fourier transform infrared spectrometer (FTIR, Nicolet 5700, Thermo Fisher, USA) detected the infrared spectrum of membranes. An X-ray diffractometer (XRD, X'Pert Pro, PANalytical, Netherland) was applied to qualitatively analyze the crystalline phase of the samples with Cu Kγ radiation at 30 mA and 30 kV. The 2θ diffraction angles of XRD were in the range of 10° and 60°, with a step size of 0.02°. A drop of Milli-Q water was placed directly on the sample using a syringe. Water contact angles on pure Ti, CMC, CMCG4, CMCG6, and CMCG8 groups ($n = 5$) were measured by CASTs 3.0 (SL200KS, KINO, USA) at room temperature.

2.4.2. Swelling ratio. Swelling characteristics of membranes were detected by soaking the samples into phosphate buffer saline (PBS) for 2, 5, 10, 20, 30, 45, 60, 90, and 120 min. The swelling ratio (S) was calculated as $S = (M_3 - M_2)/(M_2 - M_1)$. In the equation, M_1 represents the weight of the pure Ti disk. In comparison, M_2 and M_3 denote the dry weight of the sample and the wet weight of the sample after being soaked in PBS for a period, respectively.

2.4.3. Degradation ratio. The degradation ratio of membranes was examined at 37 °C in 1.5 mM lysozyme, with sterilized PBS. At a specific time point (6 h, 12 h, 1 d, 2 d, 3 d, 7 d, 14 d, 21 d, and 28 d), samples were rinsed and desiccated for 1 d at room temperature. After being weighed, the disk was placed back into the original soaking solution. W_1, W_2, and W_3 were pure Ti disks, the dry weights of samples, and wet weights after fixed time intervals, respectively. The mass loss percentage (M) represents the degradation ratio of composite membranes *in vitro*, which was calculated as $M = (W_2 - W_3)/(W_2 - W_1)$.

2.5. *In vitro* cytological study

2.5.1. Cell culture and inoculation. A 6 week-old male Wistar rat was sacrificed to extract the bone mesenchymal stem cells (BMSCs). To maintain the BMSCs, a medium composed

with Alpha Minimal Essential Medium (α-MEM, HyClone, USA), 10% Fetal Bovine Serum (FBS, Tianhang Biotechnology, China), 1% Penicillin/Streptomycin Solution (Gibco, Thermo Fisher, USA) was pre-made. Cells were incubated at 37 °C in an atmosphere of 5% CO_2. BMSCs were trypsinized and re-suspended when they had covered 80% of the culture flask bottom. To conduct cytological testing, all specimens were autoclaved, placed in sterile 24-well plates, then immersed with 1 mL pre-made medium for 24 h. Afterward, cells were inoculated at a density of 2×10^5 cells per well and incubated in the extracted solution. The medium was exchanged every day. A cell counter (Vi-CELL XR, Beckman Coulter, USA) was used for cell counting.

2.5.2. Cell adhesion and viability. Samples of pure Ti, CMC, CMCG4, CMCG6, and CMCG8 groups were cultured with cells for 1 d, then fixed with 4% paraformaldehyde for 10 min. After rinsing with PBS, 0.5% Triton X-100 solution was applied for 5 min to permeabilize the cells. Specimens were soaked in 1% bovine serum albumin (PBS solvent) for 30 min. Rhodamine–phalloidin (R-415 kit, Invitrogen, USA) was used to stain the cytoskeletons of BMSCs for 30 min at room temperature. In addition, 4′,6-diamidino-2-phenylindole (DAPI, Invitrogen, Switzerland) was used to stain the nuclei of BMSCs. Then, they were mounted for 2 h in the dark at room temperature and observed with a fluorescence microscope (TE-2000, Nikon, Japan).

To observe the cell surface morphology, specimens were rinsed with PBS three times and then fixed with pre-cooled 4% paraformaldehyde for 60 min and at 4 °C after 1 d of culture. When samples were thoroughly re-rinsed with PBS, they were dehydrated by a sequence of gradient ethyl alcohol. Finally, samples were gold-sputtered and observed by SEM.

In addition to cell adhesion, a Cell Counting Kit-8 (CCK-8, Dojindo, Japan) was used to detect cell viability. Briefly, the culture medium was exchanged with 400 mL 10% CCK-8 solution (pre-made culture medium as the solvent) in the dark after being cultured for 1, 4, and 7 days. Specimens were then cultured for 60 min at 37 °C, and the absorbance of the mixture was detected with a microplate reader (Powerwave XS2, Biotec, UK) at 450 nm.

2.5.3. Cell apoptosis. Cell apoptosis was detected by the Annexin V-FITC/PI double staining kit (Vazyme Biotech, China). BMSCs cultured as above were processed with trypsin without EDTA, then centrifuged and rinsed with pre-cooling PBS. Then, they were recollected at a cell density of 5×10^5 cells per mL. Afterward, they were re-suspended in 100 μL binding buffer. 5 μL of each Annexin V-FITC and propidium iodide (PI) was applied to stain the cells for 10 min at room temperature in the dark. 400 μL binding buffer was then blended gently. Samples of the mixture were detected by flow cytometry (CytoFlex S, Beckman Coulter, USA) at 488 nm.

2.6. Statistical analysis

Quantitative data are reported as means ± standard deviation. One-way analysis of variance was applied for all the calculations. $p < 0.05$, $p < 0.01$, and $p < 0.001$ was expressed by *, **, and ***, respectively. Among them, $p < 0.05$ was considered statistically significant.

3. Results and discussion

3.1. Characterization of grouping

CMC could modulate physical and biological properties, such as chelating, sorption, moisture retention, cell functioning antioxidant, antibacterial, antiapoptotic, *etc*.[17] Compared to chitosan, CMC has better aqueous solubility, controllable biocompatibility, and osteogenetic induction potential.[18] CMC is composed of natural biomacromolecules with negative charges. Therefore, AED, instead of the traditional CED, is applicable. The type B gelatin was chosen because it was derived from an alkaline medium. It was reported that type B gelatin nanoparticles could entrap the negative-charged sericin to a great extent.[19] Sericin is a protein created by *Bombyx mori* in the production of silk. The introduction of type B gelatin could aid sericin in contributing to the formation of membranes and help improve its biological functions. Although there is a repulsive force between negatively charged sericin and type B gelatin molecules. The results have verified that the electric field and intermolecular forces are large enough to deposit both molecules on the anode.

Regarding the amount of CMC and gelatin, we initially chose the ratio of 3/7 based on our previous study.[12] However, when we continued to increase the gelatin content, we found the membranes were more easily fabricated, and the cell biocompatibility was better. Consequently, the CMCG ratios of the CMCG4, CMCG6, and CMCG8 groups were 4/10, 4/15, and 4/20 (shown in Table 1).

3.2. Characterization of membranes

Fig. 1A–E shows the images of pure Ti and membranes. As shown in Fig. 1B, the membrane of CMC was heterogeneous, and the size of pores ranged from 100 to 200 μm. The generation of pores came from the gas formation at the anode, which trapped the hydrogen bubbles in the membranes during the

Table 1 The concentration of the AED solution and related detection results of the freshly fabricated samples ($n = 3$)

Formulation	CMC	CMCG4	CMCG6	CMCG8
CMC (mg)	320	320	320	320
Gelatin (g)	0	0.8	1.2	1.6
Milli-Q water (mL)	20	20	20	20
pH of samples	4.77.0 ± 0.22	4.06 ± 0.15	3.95 ± 0.08	3.96 ± 0.17
Zeta potential (mV)	−28.03 ± 3.28	−19.93 ± 1.23	−16.60 ± 0.71	−15.78 ± 0.33

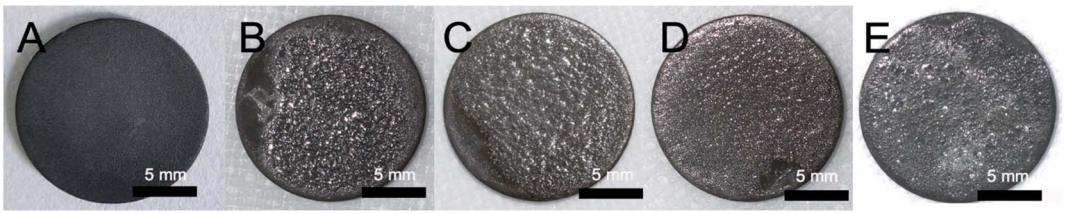

Fig. 1 Photographs of the freshly-made wet specimens: (A) pure Ti (B) CMC (C) CMCG4 (D) CMCG6 (E) CMCG8.

deposition process.[20] However, after exposure to the gelatin mixture, the membranes became dense because the gelatin foam was composed of closed pores with an average pore size of about 100 μm.[21] Therefore, as the distribution of pores became regular, their diameters also became smaller. In addition, the higher the concentration of gelatin in the AED solution, the more the amount of gelatin ionized, which makes the membrane denser.[22]

The pH value of each sample of the CMC, CMCG4, CMCG6, and CMCG8 groups was measured. As Table 1 showed, the pH value of CMC membranes was 5.0. With the addition of gelatin, the pH value tended to be more acidic, perhaps because the isoelectric point of type B gelatin is less than 7.0. Acidic surfaces would help cell adhesion because the cytomembrane surface is negatively charged.[23]

The zeta potentials of solutions are shown in Table 1. According to the table, the zeta potential of the CMC solution was -28.03 ± 3.28 mV. With the addition of gelatin, a macromolecular hydrophilic organic substance, the zeta potential became lower, and the particle dispersion system became more unstable. The zeta potential of colloids is critical in the process of deposition. It was essential to stabilize the suspension by confirming the direction of particle migration and the intensity of repulsive interactions.[24] In addition, the lowest zeta potential was -15.78 ± 0.33 mV, and it was still high enough to fabricate CMCG membranes.

As shown in Fig. 2, the characteristic peak of CMC is located in 1 rs in the C6 position.[25] The peaks around 1408 and 1581 cm^{-1} were originated from –COOH asymmetrical and symmetrical stretching vibration, respectively.[26] With the addition of gelatin, some functional groups, such as –CONH– or –NH– were introduced. Consequently, there were some new peaks at 1238, 1544, and 1630 cm^{-1}, originating from C–N stretching vibration, –CONH– stretching vibration, and –NH– bending vibration,[27] respectively. This corresponded with the molecular structure of gelatin. It is apparent that as the amount of gelatin increased, the peaks inclined to decrease, as they moved from 1058 cm^{-1} of CMCG4 to 1074 cm^{-1} of CMCG6, probably due to hydrogen bonds. The disappearance of the peak at 1581 cm^{-1} may be due to the reactions between the carboxyl groups of CMC and the peptide bonds or amino groups of gelatin. New functional groups, such as peptide bonds, have been generated. In addition, since the gelatin content is much higher than that of CMC. Therefore, the peak of the carboxyl group is replaced by the peaks of the peptide bond and the amino group.

The XRD results (Fig. 3) showed a distinct peak at 2θ around 20° in the spectrum of CMC powder, and the peak of the other four groups tended to be low and broad.[28] By contrast, the 2θ peaks appeared at 26.2°, 35.1°, 38.4°, 40.2°, and 54.4° appeared. We referred to previous reports and found these peaks corresponded to Ti substrate.[12] It has been reported that the characteristic peak of gelatin was also at 20°.[29] Hence, according to XRD results, it is difficult to distinguish these groups.

Fig. 4 shows the contact angles of all five groups. The former two groups were statistically different from others. The surfaces of pure Ti were highly hydrophilic. However, as the gelatin content increased, the contact angle became larger. Oddly, CMC and gelatin were thought to be hydrophilic.[30] We speculated that hydrophilic –COOH groups of CMC have reacted with the

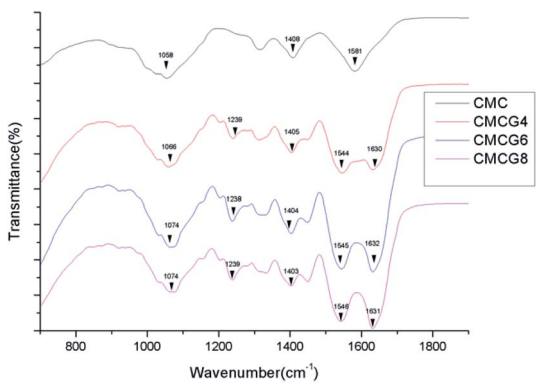

Fig. 2 FTIR spectra of the samples.

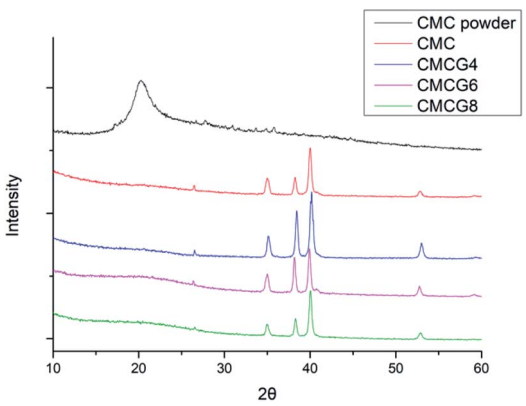

Fig. 3 XRD patterns of CMC powder, CMC, and gelatin-containing membranes.

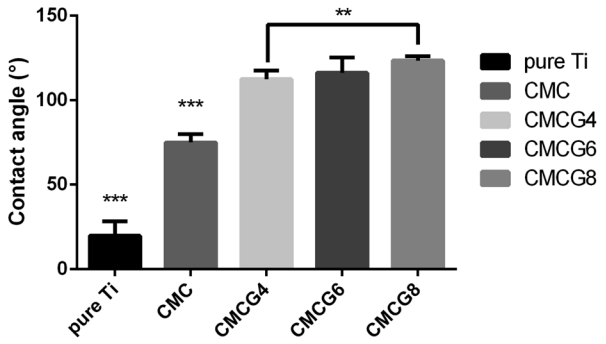

Fig. 4 Water contact angles of pure Ti and various membranes ($n = 5$).

–CONH or –NH– of gelatin. The reduction of hydrophilic groups leads to an increase in the hydrophobicity of the membrane surface, which is manifested as an increase in the water contact angle.[31] Hydrophilic surfaces are probably playing essential roles in notarizing biomedical applications. However, the combination with different properties such as super hydrophilicity could widen a new horizon in cell viability control.[32] Moreover, BMSCs could attach and stretch well as depicted in Fig. 6–8.

3.3. Swelling ratio

Swelling ratios of all samples increased to around 150% in about 30 min (Fig. 5A). Afterward, they diminished progressively and stayed steady at about 140%. A possible explanation for these results may be that the membrane volume swelled to a certain extent so that a portion of the membrane ruptured in the water. It is worth noting that the swelling ratio of the CMC group peaked at 30 min. However, with the addition of gelatin, the peak time started to be delayed until 60 min, as the swelling ratio increased further. In addition, the swelling ratios of CMCG6 and CMCG8 groups in 120 min were higher than in the initial dry samples, which were different from the CMC and CMCG4 groups. It was reported that gelatin is more absorbent than CMC.[33] Therefore, this corresponded to the results showing that incorporating gelatin with organic CMC membranes could significantly impact swelling. All membranes in the dry state could swell nearly twice in mass after being soaked in PBS solution. Because of the increased volume, the membranes covered tiny interspaces around the implant, which was essential for the stabilization.[34]

3.4. Degradation ratio

As shown in Fig. 5B, the mass of all specimens diminished dramatically in the first week, then diminished afterwards with a relatively minor change. Upon termination, the mass loss in the CMC, CMCG4, CMCG6, and CMCG8 group was 72.9 ± 3.1%, 76.9 ± 6.1%, 81.3 ± 2.5%, and 86.4 ± 3.6%, respectively. Notably, the degradation ratio rose as the mass of gelatin increased. It is reported that gelatin might be more easily to be degraded in the surroundings of water and lysozyme than CMC.[35] The biodegraded membranes could have transient properties, starting solid and supportive and degrading over

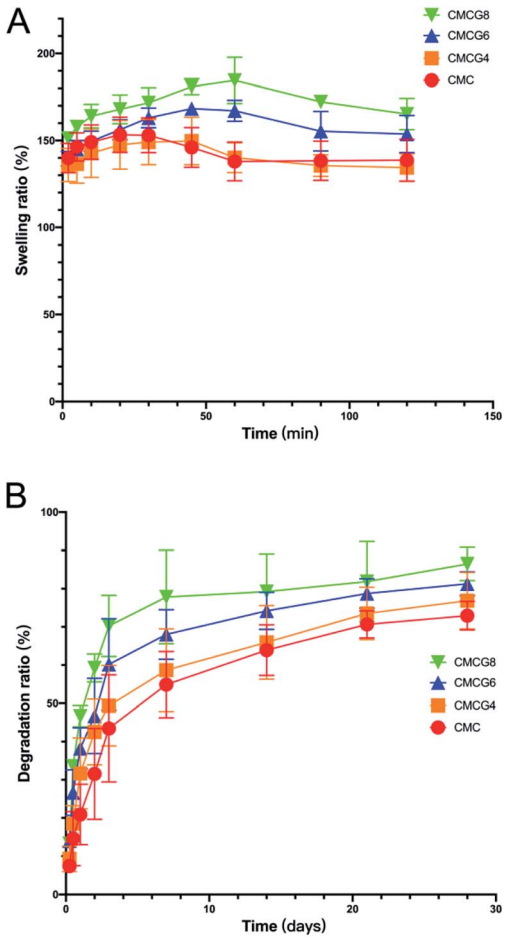

Fig. 5 (A) Swelling ratio among membranes of the five groups. (B) Degradation ratio among membranes of the five groups.

time to give the newly formed bone room to grow in the area of the membranes.[36]

3.5. *In vitro* cytological study

3.5.1. Cell adhesion and viability. Fluorescence microscopy images of the cytoskeleton cultivated on diverse samples are shown in Fig. 6. BMSCs in all five groups showed stretched cells and orderly cytoskeleton. Membranes became thicker and denser as the gelatin content increased and more cells were covered. The thicker membranes may increase the swelling ratio and prolong the release of loaded agents.[37] However, thicker membranes could also delay biodegradation time and induce more defects such as cracks.[38] No group of membranes exhibited erratic morphologies with few filopodia and cellular interactions. This substantiated that CMC and gelatin did not harm BMSCs.

We further observed the cell surface morphology by SEM (Fig. 7). In all five groups, cells presented regular shuttle shapes. In Fig. 7B, G, L and Q, a number of filopodia are observed. Filopodia and lamellipodia play critical roles in environment-sensing and cell guidance.[39] Prolonged lamellipodia and filopodia could also promote the cell anchoring into the

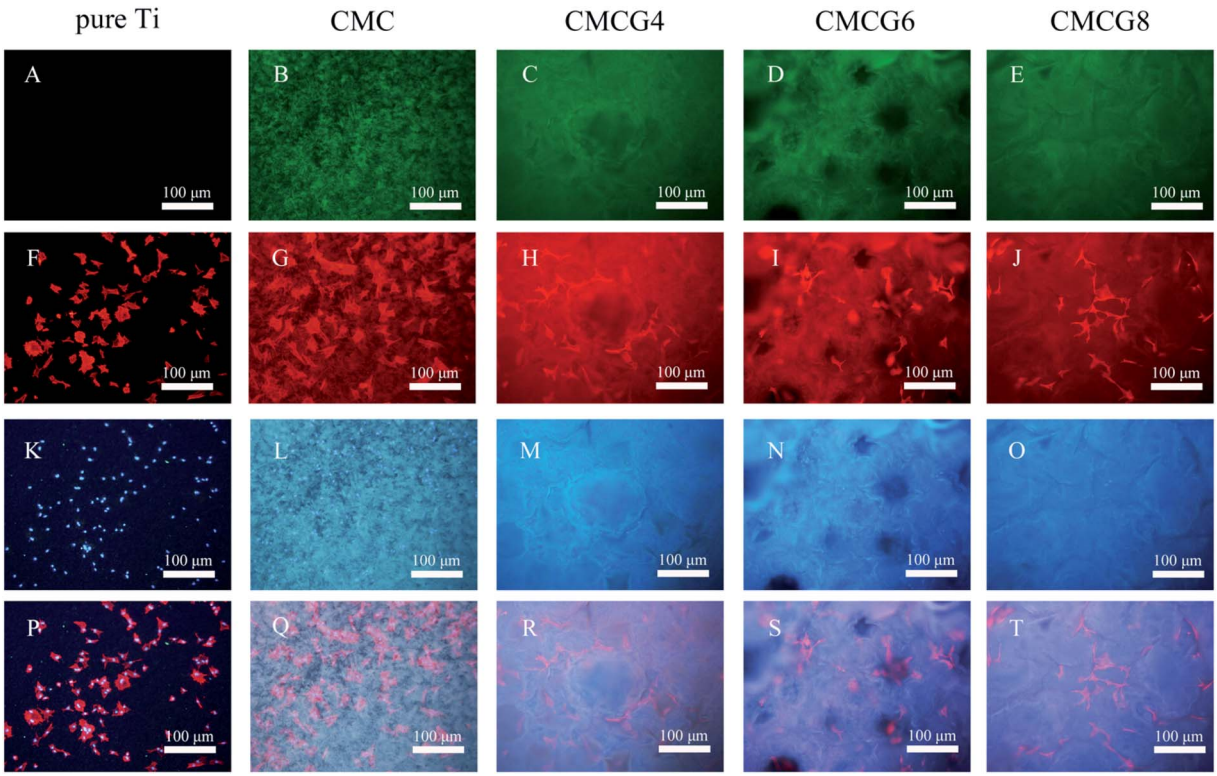

Fig. 6 Fluorescence microscopy images of membranes and cytoskeletons of BMSCs. (A–E) Pure Ti, CMC, and CMC/G samples showed green fluorescence. (F–J) Cytoskeletons stained with rhodamine–phalloidin showed red fluorescence. (K–O) The nuclei stained with DAPI showed blue fluorescence. (P–T) The merged images of nuclei, cytoskeletons, and membranes.

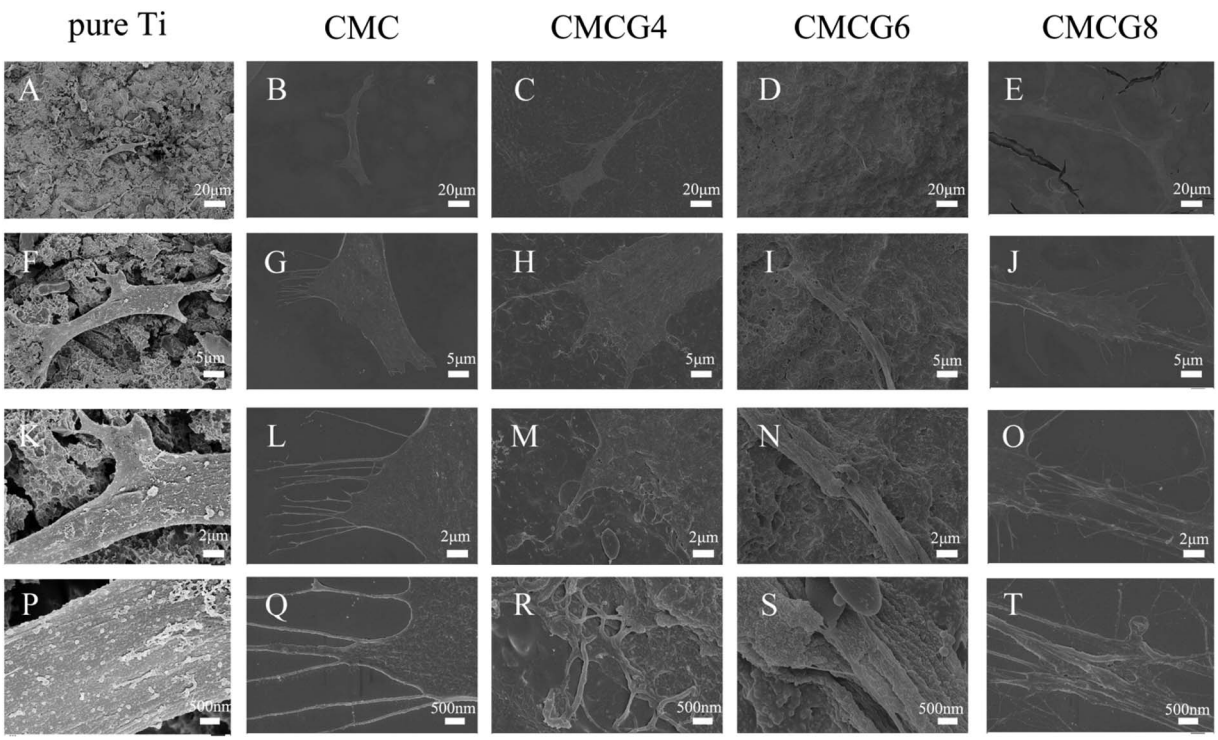

Fig. 7 The SEM images of BMSCs after being cultured with samples of pure Ti (A, F, K, and P), CMC (B, G, L, and Q), CMCG4 (C, H, M, and R), CMCG6 (D, I, N, and S), and CMCG8 (E, J, O, and T) in different magnifications.

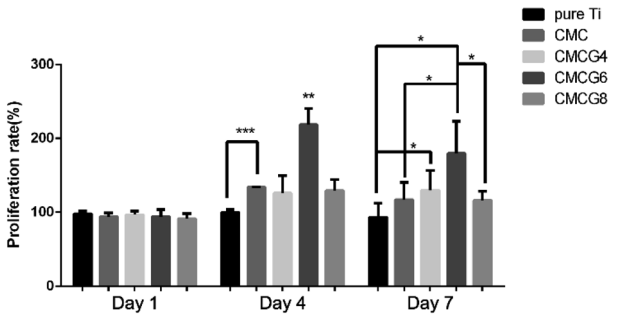

Fig. 8 The cell proliferation rate of BMSCs co-cultured with the samples of pure Ti, CMC, CMCG4, CMCG6, and CMCG8.

membranes. It was reported that filopodial traction could induce lamellipodial extension, which implied that the synergetic cooperation between filopodia and lamellipodia plays a vital role in cell anchoring.[40] Therefore, filopodia and lamellipodia could be an index of cell viability.[41]

The cell viabilities of cells in pure Ti, CMC, CMCG4, CMCG6, and CMCG8 groups by CCK-8 at specific intervals are shown in Fig. 8. There were no apparent differences among the five groups on the first day. After 3 days, the proliferation rate of the CMC group was significantly different from the negative controlled group pure Ti. That of the CMCG6 group was significantly different from that of the other four groups. On the seventh day, we could see the CMCG6 group still had the highest proliferation rate, significantly different from the pure Ti group and CMCG8 group. In addition, the proliferation rate of the CMCG4 group was also higher than the rate of the negative control group pure Ti. Cell adhesion and viability results might explain how BMSCs have a significant proliferative effect on any samples.[42]

CMC has been actively studied as a chitosan derivative because of its physicochemical and biological properties, such as biocompatibility and superior bio-adhesive properties.[43] It could also maintain the scaffold structure and enhance the cell viability of chondrocytes.[44] It has been reported that gelatin possesses excellent biocompatibility, easy biodegradability, and weak antigenicity.[45] Moreover, as in the report of our previous study, the addition of gelatin could enhance the biocompatibility of membranes.[12] This explains why the proliferation rates of the CMCG4 and CMCG6 groups were statistically higher. However, an excess amount of gelatin would impact the proliferation rate of cells, which was reflected in the result of group CMCG8 shown in Fig. 8.

3.5.2. Cell apoptosis. Quantitative analysis of Annexin V-FITC/PI staining was carried out to assess the different periods of apoptosis. In Fig. 9A, the upper and lower left quadrants show the percentage of necrotic or viable cells. The upper and lower right quadrants show the proportion of late and early apoptotic cells, respectively.

As shown in Fig. 9B, the apoptosis rate among the five groups was not precisely the same. The CMC group showed the lowest apoptosis rate. With the addition of gelatin, the apoptosis rate was increased.

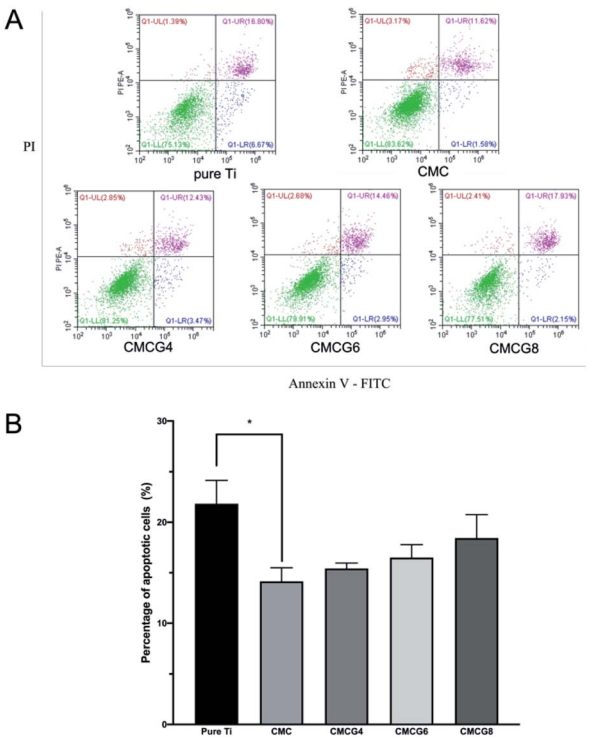

Fig. 9 Apoptotic conditions of BMSCs stained with Annexin V-FITC/PI. (A) Flow cytometric analysis of apoptotic BMSCs on various samples. (B) Percentages of apoptotic cells among different groups ($n = 3$).

It has been reported that CMC could inhibit cell apoptosis and restore the reduction of the mitochondrial membrane potential in chondrocytes.[46] CMC could also protect chondrocytes from interleukin-1β-induced apoptosis.[47] In addition, as a commonly used biomaterial with good biocompatibility, there is no report on the relationship between gelatin alone and cell apoptosis. We assumed that a large amount of gelatin could offset part of CMC's ability to inhibit cell apoptosis.

Apoptosis is an inflammatory trigger that could reduce the pathogens and repair the damage during infection. However, it could cause a suppressive, protective, or autoreactive immune response.[48] Consequently, we found that the cell apoptosis of BMSCs influenced all five groups. And the CMC group presented the lowest late apoptosis rate. Moreover, the late apoptosis rates became higher because of the decrease in the CMC ratio. There is no report about the relation between gelatin and cell apoptosis. The abnormal result in this experiment still needs to be further studied.

4. Conclusions

This study showed that composite CMCG membranes were successfully deposited on Ti substrates. CMCG membranes showed good swelling and biodegradation characteristics and were hydrophobic to some degree. For *in vitro* experiments, the membranes were biocompatible and could enhance cell proliferation. Moreover, these membranes could inhibit cell apoptosis in BMSCs. Therefore, it could possible to

functionalize the surface of Ti substrates with CMCG membranes *via* an economical, eco-friendly, and convenient synthesis method, AED. This technique could also be used as a carrier to load more medical agents with negative charges and play a role against infection.

Conflicts of interest

The authors declare that they have no known competing financial interests or personal relationships that could have influenced the work reported in this paper.

Acknowledgements

We gratefully acknowledge the financial support of the National Natural Science Foundation of China (No. 81470771, 81901063), the Fundamental Research Funds for the Central Universities (No. 2042017kf0075, 2042020kf0189), and the Doctoral Fund of the Ministry of Education of China (No. 20120141130009).

References

1 M. Rakic, P. Galindo-Moreno, A. Monje, S. Radovanovic, H.-L. Wang, D. Cochran, A. Sculean and L. Canullo, *Clin. Oral Investig.*, 2018, **22**, 1805–1816.
2 K. C. Popat, M. Eltgroth, T. J. Latempa, C. A. Grimes and T. A. Desai, *Biomaterials*, 2007, **28**, 4880–4888.
3 F. Schwarz, J. Derks, A. Monje and H. L. Wang, *J. Periodontol.*, 2018, **89**(1), S267–S290.
4 L. Zhao, P. K. Chu, Y. Zhang and Z. Wu, *J. Biomed. Mater. Res., Part B*, 2009, **91**, 470–480.
5 K. Robertson, T. Shahbazian and S. P. R. Macleod, *Dent. Clin. North Am.*, 2015, **59**, 329–343.
6 R. Smeets, B. Stadlinger, F. Schwarz, B. Beck-Broichsitter, O. Jung, C. Precht, F. Kloss, A. Gröbe, M. Heiland and T. Ebker, *BioMed Res. Int.*, 2016, **2016**, 6285620.
7 D. M. Campos, K. Gritsch, V. Salles, G. N. Attik and B. Grosgogeat, *BioRes. Open Access*, 2014, **3**, 117–126.
8 L. Caseli, R. P. Cavalheiro, H. B. Nader and C. C. Lopes, *Biochim. Biophys. Acta*, 2012, **1818**, 1211–1217.
9 D. Schwartzman, A. W. Pasculle, K. D. Ceceris, J. Smith, L. E. Weiss and P. G. Campbell, *Biomaterials*, 2015, **60**, 1–8.
10 P. Bajaj, R. M. Schweller, A. Khademhosseini, J. L. West and R. Bashir, *Annu. Rev. Biomed. Eng.*, 2014, **16**, 247–276.
11 A. Sorkio, P. J. Porter, K. Juuti-Uusitalo, B. J. Meenan, H. Skottman and G. A. Burke, *Tissue Eng., Part A*, 2015, **21**, 2301–2314.
12 T. Jiang, Z. Zhang, Y. Zhou, Y. Liu, Z. Wang, H. Tong, X. Shen and Y. Wang, *Biomacromolecules*, 2010, **11**, 1254–1260.
13 K. Ma, D. Huang, J. Cai, X. Cai, L. Gong, P. Huang, Y. Wang and T. Jiang, *Colloids Surf., B*, 2016, **146**, 97–106.
14 O. Rzhepishevska, S. Hakobyan, R. Ruhal, J. Gautrot, D. Barbero and M. Ramstedt, *Biomater. Sci.*, 2013, **1**, 589–602.
15 L. Upadhyaya, J. Singh, V. Agarwal and R. P. Tewari, *Carbohydr. Polym.*, 2013, **91**, 452–466.
16 Q. Chen, U. D. Larraya, N. Garmendia, M. Lasheras-Zubiate, L. Cordero-Arias, S. Virtanen and A. R. Boccaccini, *Colloids Surf., B*, 2014, **118**, 41–48.
17 V. Mourya, N. N. Inamdar and A. Tiwari, *Adv. Mater. Lett.*, 2010, **1**, 11–33.
18 L. Upadhyaya, J. Singh, V. Agarwal and R. P. Tewari, *J. Controlled Release*, 2014, **186**, 54–87.
19 P. Aramwit, N. Jaichawa, J. Ratanavaraporn and T. Srichana, *Mater. Express*, 2015, **5**, 241–248.
20 D. Huang, K. Ma, X. Cai, X. Yang, Y. Hu, P. Huang, F. Wang, T. Jiang and Y. Wang, *Int. J. Nanomed.*, 2017, **12**, 7483.
21 S. M. Lien, L. Y. Ko and T. J. Huang, *Acta Biomater.*, 2009, **5**, 670–679.
22 S. Lebrette, C. Pagnoux and P. Abelard, *J. Eur. Ceram. Soc.*, 2006, **26**, 2727–2734.
23 B. P. Orner, R. Derda, R. L. Lewis, J. A. Thomson and L. L. Kiessling, *J. Am. Chem. Soc.*, 2004, **126**, 10808–10809.
24 M. Zarbov, I. Schuster and L. Gal-Or, *J. Mater. Sci.*, 2004, **39**, 813–817.
25 K. Koshiji, Y. Nonaka, M. Iwamura, F. Dai, R. Matsuoka and T. Hasegawa, *Carbohydr. Polym.*, 2016, **137**, 277–286.
26 Y. Cheng, Z. Hu, Y. Zhao, Z. Zou, S. Lu, B. Zhang and S. Li, *Int. J. Mol. Sci.*, 2019, **20**, 3980.
27 K. J. Payne and A. Veis, *Biopolymers*, 1988, **27**, 1749–1760.
28 P. Moganavally, M. Deepa, P. Sudha and R. Suresh, *Orient. J. Chem.*, 2016, **32**, 441.
29 L. Radev, M. Fernandes, I. Salvado and D. Kovacheva, *Open Chem.*, 2009, **7**, 721–730.
30 F. Wang, P. Huang, D. Huang, Y. Hu, K. Ma, X. Cai and T. Jiang, *J. Mater. Chem. B*, 2018, **6**, 2304–2314.
31 W. Geng, S. Liu, J. Guo and L. Zhang, *J. Mol. Liq.*, 2019, **276**, 638–643.
32 M. Ferrari, F. Cirisano and M. C. Morán, *Colloids Interfaces*, 2019, **3**, 48.
33 A. Shukla, J. C. Fang, S. Puranam and P. T. Hammond, *J. Controlled Release*, 2012, **157**, 64–71.
34 J. Raphel, M. Holodniy, S. B. Goodman and S. C. Heilshorn, *Biomaterials*, 2016, **84**, 301–314.
35 C. Yang, L. Xu, Y. Zhou, X. Zhang, X. Huang, M. Wang, Y. Han, M. Zhai, S. Wei and J. Li, *Carbohydr. Polym.*, 2010, **82**, 1297–1305.
36 O. Böstman and H. Pihlajamäki, *Biomaterials*, 2000, **21**, 2615–2621.
37 Q. Tian, J. Lin, L. Rivera-Castaneda, A. Tsanhani, Z. S. Dunn, A. Rodriguez, A. Aslani and H. Liu, *Sci. Rep.*, 2019, **9**, 1–27.
38 I. Johnson, J. Lin and H. Liu, *Orthopedic Biomaterials*, 2017, pp. 331–363.
39 R. You, X. Li, Z. Luo, J. Qu and M. Li, *Biointerphases*, 2015, **10**, 011005.
40 R. You, X. Li, Y. Liu, G. Liu, S. Lu and M. Li, *J. Biomed. Mater. Res., Part A*, 2014, **102**, 4206–4212.
41 A. Arjonen, R. Kaukonen and J. Ivaska, *Cell Adhes. Migr.*, 2011, **5**, 421–430.
42 B. Uslu, B. Biltekin, S. Denir, S. Özbaş-Turan, S. Arbak, J. Akbuğa and A. Bilir, *Biotech. Histochem.*, 2016, **91**, 20–29.
43 Z. Shariatinia, *Int. J. Biol. Macromol.*, 2018, **120**, 1406–1419.

44 F. Han, X. Yang, J. Zhao, Y. Zhao and X. Yuan, *J. Mater. Sci.: Mater. Med.*, 2015, **26**, 160.
45 D. Liu, M. Nikoo, G. Boran, P. Zhou and J. M. Regenstein, *Annu. Rev. Food Sci. Technol.*, 2015, **6**, 527–557.
46 L. Jiang, Y. Liu, M.-M. Ma, Y.-B. Tang, J.-G. Zhou and Y.-Y. Guan, *Apoptosis*, 2013, **18**, 556–565.
47 Q. Chen, S.-Q. Liu, Y.-M. Du, H. Peng and L.-P. Sun, *Eur. J. Pharmacol.*, 2006, **541**, 1–8.
48 M. B. Torchinsky, J. Garaude and J. M. Blander, *Curr. Opin. Immunol.*, 2010, **22**, 55–62.